

Cite this: *Dalton Trans.*, 2020, **49**,  
2527

# Molecular enneanuclear Cu<sup>II</sup> phosphates containing planar hexanuclear and trinuclear sub-units: syntheses, structures, and magnetism†‡

Biswajit Santra,<sup>a</sup> Pankaj Kalita,<sup>b</sup> Shubhadeep Chandra,<sup>c,d</sup> Debdeep Mandal,<sup>a</sup> Vierandra Kumar,<sup>e</sup> Ramakirushnan Surya Narayanan,<sup>a</sup> Atanu Dey,<sup>b</sup> Nicolas Chrysochos,<sup>f</sup> Volker Huch,<sup>g</sup> Sourav Biswas,<sup>h</sup> Debajyoti Ghoshal,<sup>\*h</sup> E. Carolina Sañudo,<sup>i,j</sup> Biprajit Sarkar,<sup>i,c,d</sup> Carola Schulzke,<sup>i,f</sup> Vadapalli Chandrasekhar<sup>i,a,e</sup> and Anukul Jana<sup>i,a</sup>

Highly symmetric enneanuclear copper(II) phosphates [Cu<sub>9</sub>(Pz)<sub>6</sub>(μ-OH)<sub>3</sub>(μ<sub>3</sub>-OH)(ArOPO<sub>3</sub>)<sub>4</sub>(DMF)<sub>3</sub>] (PzH = pyrazole, Ar = 2,6-(CHPh<sub>2</sub>)<sub>2</sub>-4-R-C<sub>6</sub>H<sub>2</sub>; R = Me, **2<sup>MeAr</sup>**; Et, **2<sup>EtAr</sup>**; iPr, **2<sup>iPrAr</sup>**; and Ar = 2,6-iPr<sub>2</sub>C<sub>6</sub>H<sub>3</sub>, **2<sup>Dip</sup>**) comprising nine copper(II) centers and pyrazole, hydroxide and DMF as ancillary ligands were synthesized by a reaction involving the arylphosphate monoester, **1**, copper(I)chloride, pyrazole, and triethylamine in a 4 : 9 : 6 : 14 ratio. All four complexes were characterized by single crystal structural analysis. The complexes contain two distinct structural motifs within the multinuclear copper scaffold: a hexanuclear unit and a trinuclear unit. In the latter, the three Cu(II) centres are bridged by a μ<sub>3</sub>-OH. Each pair of Cu(II) centers in the trinuclear unit are bridged by a pyrazole ligand. The hexanuclear unit is made up of three dinuclear Cu(II) motifs where the two Cu(II) centres are bridged by an -OH and a pyrazole ligand. The three dinuclear units are connected to each other by phosphate ligands. The latter also aid the fusion of the trinuclear and the hexanuclear motifs. Magnetic studies reveal a strong antiferromagnetic exchange between the Cu(II) centres of the dinuclear units in the hexanuclear part and a strong spin frustration in the trinuclear part leading to a degenerate ground state.

Received 29th November 2019,

Accepted 17th January 2020

DOI: 10.1039/c9dt04584h

rsc.li/dalton

## Introduction

Metallophosphates/phosphonates possessing extended structures have been studied considerably in view of their potential applications as ion exchangers,<sup>1</sup> fast-ion conductors,<sup>2–5</sup> catalysts,<sup>6–12</sup> adsorption materials,<sup>13,14</sup> matrices for electronic devices,<sup>15,16</sup> photoluminescent materials,<sup>17–19</sup> biomaterials,<sup>20–23</sup> gas storage materials and magnetic materials.<sup>24–26</sup> In contrast, studies on the molecular analogues

of these systems have been stymied by synthetic challenges. One such challenge, due to the multi-functional nature of the ligands, is to prevent the formation of coordination polymeric networks and thus direct the reaction towards the molecular analogues. We and others have developed several strategies towards realizing this goal.<sup>27–31</sup> This includes use of ancillary ligands, sterically hindered phosphorus-acid ligands *etc.* While these strategies have been quite successful with molecular transition metal phosphonates in which the nuclearity could

<sup>a</sup>Tata Institute of Fundamental Research Hyderabad, Gopanally, Hyderabad-500107, India. E-mail: ajana@tifrh.res.in

<sup>b</sup>National Institute of Science Education and Research Bhubaneswar, HBNI, Bhubaneswar-752050, Odisha, India

<sup>c</sup>Institut für Chemie und Biochemie, Anorganische Chemie, Freie Universität Berlin, Fabeckstraße 34–36, 14195 Berlin, Germany. E-mail: biprajit.sarkar@fu-berlin.de

<sup>d</sup>Institut für Anorganische Chemie, Universität Stuttgart, Pfaffenwaldring 55, D-70569 Stuttgart, Germany. E-mail: biprajit.sarkar@iac.uni-stuttgart.de

<sup>e</sup>Department of Chemistry, Indian Institute of Technology Kanpur, Kanpur 208016, India. E-mail: vc@iitk.ac.in

<sup>f</sup>Institut für Biochemie, Universität Greifswald, Felix-Hausdorff-Straße 4, D-17487 Greifswald, Germany. E-mail: carola.schulzke@uni-greifswald.de

<sup>g</sup>Krupp-Chair of General and Inorganic Chemistry, Saarland University, 66123 Saarbrücken, Germany

<sup>h</sup>Department of Chemistry, Jadavpur University, Jadavpur, Kolkata-32, India.

E-mail: dghoshal@chemistry.jdvu.ac.in

<sup>i</sup>Departament de Química Inorgànica i Orgànica, Secció de Química Inorgànica, Facultat de Química, Universitat de Barcelona, Diagonal 645, 08028 Barcelona, Spain. E-mail: esanudo@ub.edu

<sup>j</sup>Institut de Nanociència i Nanotecnologia, Universitat de Barcelona, Diagonal 645, 08028 Barcelona, Spain

† Dedicated to Professor G. K. Lahiri on the occasion of his 60th birthday.

‡ Electronic supplementary information (ESI) available: Molecular structures of **2<sup>EtAr</sup>** and **2<sup>iPrAr</sup>**, UV/vis and emission spectra, thermogravimetric analysis, HRMS data, FT-IR data, and CHN data (PDF). CCDC 1835293 (**2<sup>Dip</sup>**), 1835294 (**2<sup>EtAr</sup>**), 1835295 (**2<sup>MeAr</sup>**), and 1835296 (**2<sup>iPrAr</sup>**). For ESI and crystallographic data in CIF. For ESI and crystallographic data in CIF or other electronic format see DOI: 10.1039/C9DT04584H

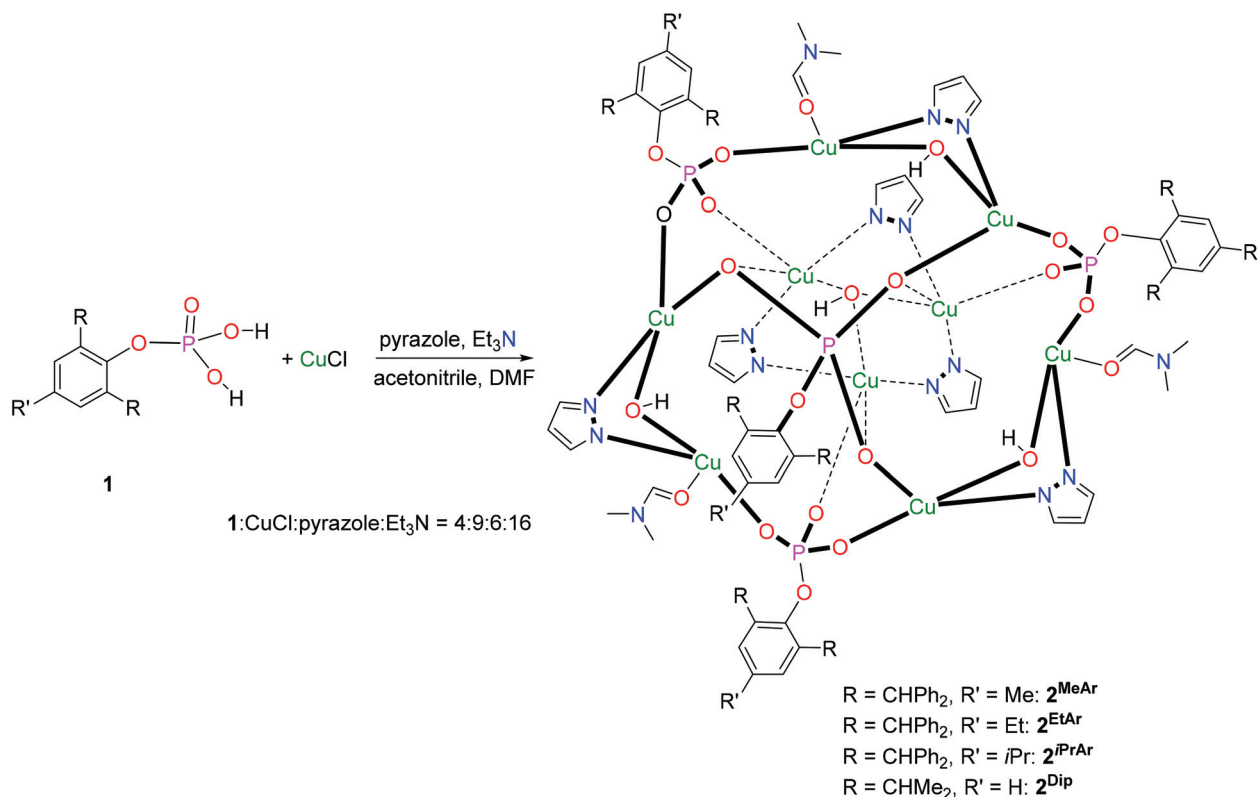
be varied over a wide range, in the case of phosphates, isolation of higher-nuclearity complexes has been limited.<sup>30,31</sup> On the other hand the phosphate ligand containing the hinge oxygen atom (separating phosphorus and the potential binding site) is likely to be more flexible and versatile. Our experience with phosphonate ligands spurred us to examine this issue more closely particularly with respect to molecular copper(II) phosphates. Besides academic interest, these copper(II) phosphates have applications that include artificial nucleases/hydrolases/phosphatases *etc.*<sup>32–35</sup> Previous efforts towards the design of molecular Cu(II) phosphates have resulted in either low-nuclearity compounds or compounds possessing polymeric structures.<sup>36,37</sup> There is a report on the isolation of a hexanuclear Cu(II) phosphate using bis(*p*-nitrophenyl)-phosphate, BNPP and pyrazole ligands.<sup>38,39</sup> Also, pyrazolate ligands are able to form copper metallacycles with diverse nuclearities.<sup>40–42</sup> In view of our successful efforts in molecular phosphonate synthesis employing ancillary pyrazole co-ligands,<sup>43–45</sup> we were interested in examining the possibility of using a sterically hindered phosphate ligand together with pyrazoles for preparing soluble, molecular, oligonuclear Cu(II) phosphate ensembles. Reported herein are investigations into the synthesis, structural, magnetic and photophysical properties of the first examples of enneanuclear Cu(II) phosphates, [Cu<sub>9</sub>(Pz)<sub>6</sub>(μ-OH)<sub>3</sub>(μ<sub>3</sub>-OH)(ArOPO<sub>3</sub>)<sub>4</sub>(DMF)<sub>3</sub>] (PzH = pyrazole, Ar = 2,6-(CHPh<sub>2</sub>)<sub>2</sub>-4-R-C<sub>6</sub>H<sub>2</sub>; R = Me, **2<sup>MeAr</sup>**; Et, **2<sup>EtAr</sup>**; iPr, **2<sup>iPrAr</sup>**; and Ar = 2,6-iPr<sub>2</sub>C<sub>6</sub>H<sub>3</sub>, **2<sup>Dip</sup>**). These complexes are made up of

two distinct sub-units: a hexanuclear part, itself consisting of three dinuclear motifs, and a trinuclear part. Magnetic studies reveal strong anti-ferromagnetism in the dinuclear motif of the hexanuclear part and the trinuclear part. In the latter, because of geometrical reasons there is a strong spin frustration resulting in a degenerate ground state.

## Results and discussion

The synthesis of enneanuclear copper(II)-phosphates was accomplished by utilizing bulky aryl substituted phosphate monoesters, ArOP(O)(OH)<sub>2</sub> where Ar = 2,6-(CHPh<sub>2</sub>)<sub>2</sub>-4-R-C<sub>6</sub>H<sub>2</sub>; R = Me, **1<sup>Me</sup>**; Et, **1<sup>Et</sup>**; iPr, **1<sup>iPr</sup>** and also the relatively less sterically hindered aryl substituted phosphate monoester DipOP(O)(OH)<sub>2</sub> where Dip = 2,6-iPr<sub>2</sub>C<sub>6</sub>H<sub>3</sub>, **1<sup>Dip</sup>**. CuCl was used as the source of copper ions and pyrazole was used as an ancillary ligand to strategically occupy one or more coordination sites on the metal so that the formation of insoluble polymeric entities could be excluded. Under optimum reaction conditions described in the Experimental section, in all cases, isostructural enneanuclear Cu(II)-metallophosphates (**2<sup>MeAr</sup>**, **2<sup>EtAr</sup>**, **2<sup>iPrAr</sup>** and **2<sup>Dip</sup>**) were isolated and crystallized from DMF solution (Scheme 1). The oxidation of copper(I) to copper(II) occurred *in situ* as the reactions were carried out under ambient conditions.

IR studies reveal characteristic stretching peaks at around 3442, 3444, 3444 and 3464 cm<sup>-1</sup> for **2<sup>MeAr</sup>**, **2<sup>EtAr</sup>**, **2<sup>iPrAr</sup>**, and **2<sup>Dip</sup>**



Scheme 1 Syntheses of Cu<sub>9</sub> clusters **2<sup>MeAr</sup>**, **2<sup>EtAr</sup>**, **2<sup>iPrAr</sup>**, and **2<sup>Dip</sup>**.

respectively, indicative of the presence of hydroxide ligands (*vide infra*). The sharp IR signals at 1145, 1147, 1147, and 1142  $\text{cm}^{-1}$  for  $2^{\text{MeAr}}$ ,  $2^{\text{EtAr}}$ ,  $2^{\text{iPrAr}}$ , and  $2^{\text{Dip}}$ , respectively, can be attributed to the coordinated P=O stretching frequency, which is slightly lower compared to the parent phosphate ligand (1172–1201  $\text{cm}^{-1}$ ) and anionic phosphate (1157–1165  $\text{cm}^{-1}$ ).<sup>46</sup> Interestingly, the absence of any absorption bands in the region of 2320–2390  $\text{cm}^{-1}$  indicates the complete deprotonation of  $1^{\text{Me}}$ ,  $1^{\text{Et}}$ ,  $1^{\text{iPr}}$  and  $1^{\text{Dip}}$  during the reaction, and hence, no P–OH groups in the product. In addition, a very sharp peak at 1642, 1642, 1641, and 1644  $\text{cm}^{-1}$  for  $2^{\text{MeAr}}$ ,  $2^{\text{EtAr}}$ ,  $2^{\text{iPrAr}}$ , and  $2^{\text{Dip}}$ , respectively, corresponds to the C=O stretching of the coordinated DMF.

### Molecular structures

Single crystal X-ray diffraction studies reveal that  $2^{\text{MeAr}}$ ,  $2^{\text{EtAr}}$ , and  $2^{\text{iPrAr}}$  crystallize in the trigonal  $R3/c$  space group, while  $2^{\text{Dip}}$  crystallizes along with additional DMF molecules in the triclinic  $P\bar{1}$  space group. All four complexes crystallize as discrete neutral complexes and essentially possess the same structural features. They are composed of nine Cu(II) centers each, plus four dianionic phosphate ligands, six pyrazolate ligands, four hydroxide ligands and three coordinated DMF molecules (see Fig. 1 for  $2^{\text{MeAr}}$  and see Fig. S1 and S2 in ESI† for the molecular structures of  $2^{\text{EtAr}}$  and  $2^{\text{iPrAr}}$ ). Even though all four compounds have grossly similar structural features,  $2^{\text{Dip}}$  exhibits some small but notable variations (Fig. 2). In view of this, we describe the structural features of  $2^{\text{MeAr}}$  below as a representative example of all compounds and detail the structural distinctions of  $2^{\text{Dip}}$  separately. Various figures visualizing and detailing the enneanuclear molecule compositions and representative metrical parameters of all four complexes are provided in the ESI (Fig. S3–S7†). In addition, to follow the discus-

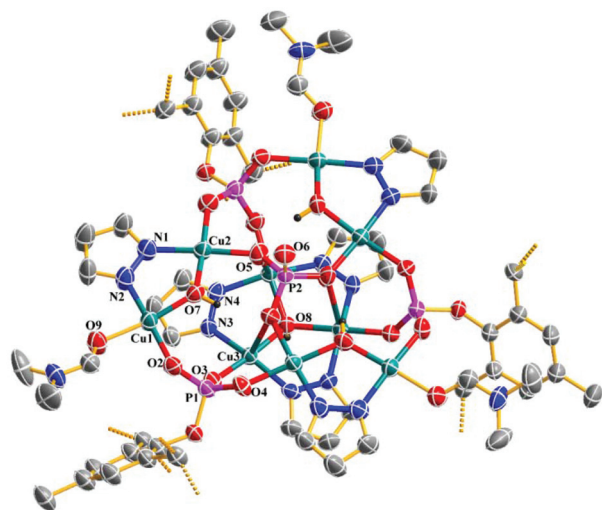


Fig. 1 Molecular structure of  $2^{\text{MeAr}}$ . The organic parts *ortho* to the phosphate moiety (represented by dotted bonds) and H-atoms (except the bridging –OH group) are omitted for clarity.

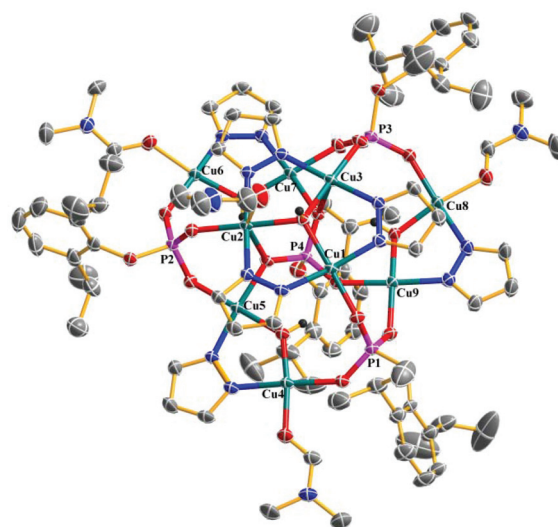


Fig. 2 Molecular structure of  $2^{\text{Dip}}$ . The organic parts *ortho* to the phosphate moiety (represented by dotted bonds) and H-atoms (except the bridging –OH group) are omitted for clarity.

sion on the connectivity of these Cu<sub>9</sub>-complexes the line diagrams of these are also provided (Fig. 3).

The enneanuclear ensemble comprises two distinct motifs: a hexanuclear moiety and a trinuclear moiety (Fig. 4). The hexanuclear building block contains three dinuclear units in which the two copper centres are bound together by means of a monodentate bridging  $\mu\text{-OH}$  and a bidentate,  $\kappa^2(\text{N},\text{N})$  pyrazolate. The dinuclear sub-units are linked to each other by the bridging coordination of a phosphate involving two of its three coordinating oxygen atoms ( $\kappa^2(\text{O},\text{O})$ ). The macrocycle, thus formed, as a result of three dimeric sub-units being connected by three phosphate ligands is an eighteen-membered macrocycle (going through the hydroxide, not the pyrazolate; the outer cycle is twenty-four-membered). Notably, the hexanuclear Cu(II) motif is planar (Fig. 4(left)). A distinction between the two copper centres in the dinuclear motif arises because one of the copper centres has a dimethyl formamide ligand and the other is bound to an oxygen atom of a capping phosphate group. Each of the copper centres is in a distorted square-planar geometry (Fig. 5(left)). A further structural inference from this inspection is that each dinuclear motif is part of a non-planar (the dihedral angle between the two planes is 11.16°) five membered ring comprising two copper centres, one oxygen (OH) and two nitrogen atoms (pyrazolate) (see Fig. S7 in ESI†). In all four compounds, the largest deviation from the mean plane describing these five atoms is found for the hydroxide oxygen atom (ranging from 0.073 Å for 2Dip to 0.246 Å for  $2^{\text{MeAr}}$ ); the other four atoms (2 Cu and 2 N) are essentially coplanar.

The trinuclear moieties of these unusual structures contain copper ions in an entirely different coordination environment in comparison to the hexanuclear moiety. In the trinuclear assembly the three Cu(II) centres are bridged by a central  $\mu_3\text{-OH}$ . Furthermore, each Cu(II) within the trinuclear unit is connected to two adjacent Cu(II) ions by two  $\kappa^2(\text{N},\text{N})$  pyrazo-

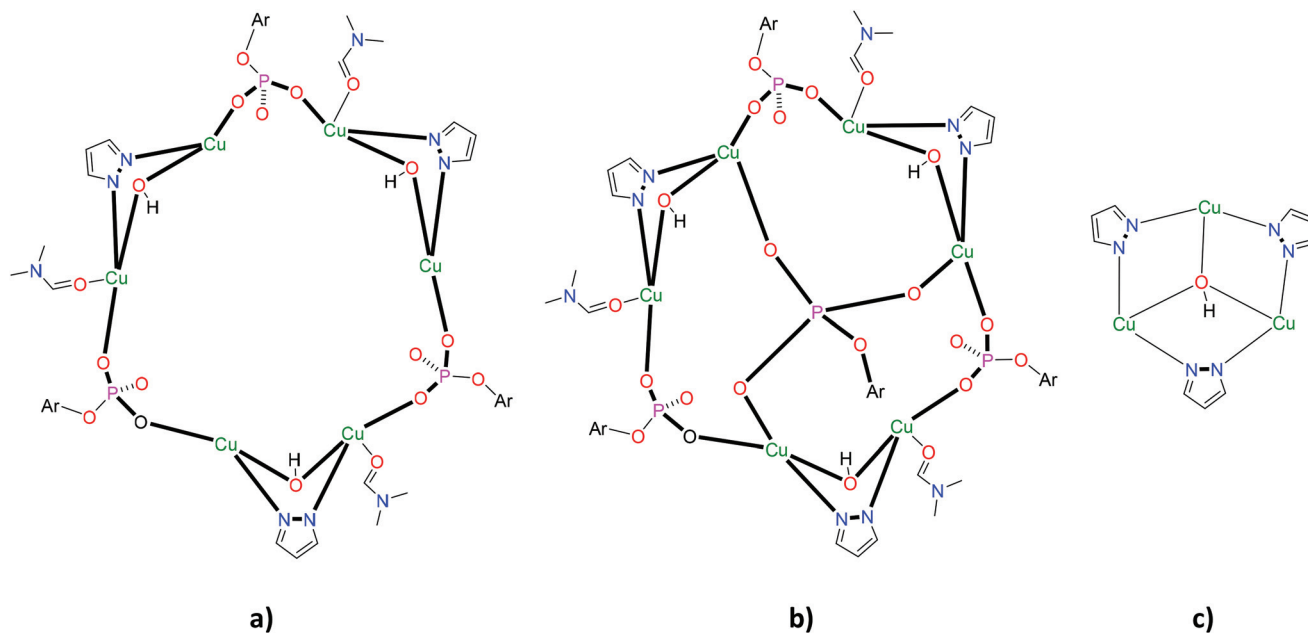


Fig. 3 Simplified line-diagrams of (a) the hexanuclear copper core without capping phosphate, (b) the hexanuclear copper core with capping phosphate, and (c) the pyrazole bridged trinuclear copper core (Ar = 2,6-(CHPh<sub>2</sub>)<sub>2</sub>-4-R-C<sub>6</sub>H<sub>2</sub>; R = Me, 2<sup>MeAr</sup>, Et, 2<sup>EtAr</sup>, iPr, 2<sup>iPrAr</sup>; and Ar = 2,6-iPr<sub>2</sub>C<sub>6</sub>H<sub>3</sub>, 2<sup>Dip</sup>).

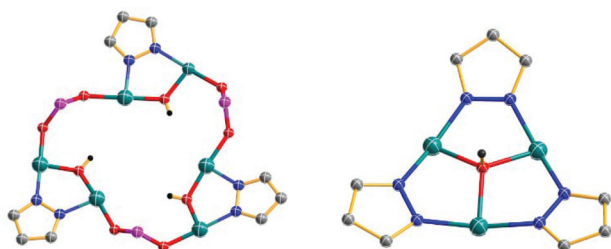


Fig. 4 The view of (a) the hexanuclear eighteen membered copper core (left) and (b) the trinuclear nine membered copper core of the 2<sup>MeAr</sup> complex (right).

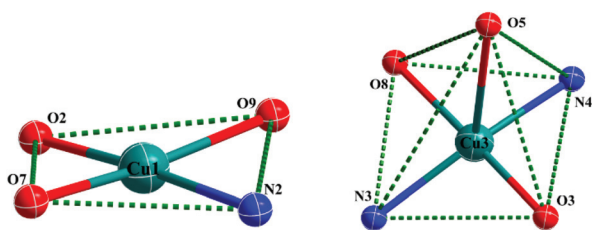


Fig. 5 View of (a) distorted square planar Cu(II) (O9 is part of coordinated DMF) (left) and (b) distorted square pyramidal Cu(II) for the 2<sup>MeAr</sup> complex (right).

lates. Such an organization leads to a nine-membered macrocycle (Fig. 4(right)) containing three non-planar five membered (2 × Cu, 1 × O, and 2 × N) rings. Again, it is the hydroxide oxygen atom which most strongly deviates from the co-planarity of the rest of the ensemble.

The trimeric motif is connected to the hexameric motif by the bridging coordination of three mono-phosphate-ester ligands. Each of these three phosphates bridge two dimeric copper units of the hexanuclear moiety with two of its free oxygen atoms and uses its third oxygen atom to bind one of the three Cu(II) centres of the trinuclear unit. The fourth phosphate of the complexes exhibits an entirely different capping binding mode by only interacting strongly with the hexanuclear moiety. Here, it binds every second copper centre in a symmetric  $\kappa^3(\text{O},\text{O},\text{O})$  fashion. A potential interaction, if at all, with the three copper centres of the trimeric motif has to be considered very weak with Cu–O distances of 2.84 Å in 2<sup>MeAr</sup>, *i.e.* 0.9 Å longer than the sum of the covalent radii. As a result of this, the overall coordination of the three Cu(II) centres of the trimeric unit is equivalent and could be considered five-coordinate (2N and 3O) if the weak apical interaction is included in a distorted square-pyramidal geometry (Fig. 5(right)).<sup>37,47</sup>

Inspection of the overall molecular symmetry reveals a  $C_3$  axis of symmetry passing exactly through the axial phosphate ligand. The bond distances associated with the Cu– $\mu$ -OH bonds are 1.867(3) and 1.883(2) Å with a Cu– $\mu$ -OH–Cu angle of 126.16(7)° (ESI Table S3<sup>†</sup>). The Cu–O bond distance associated with the  $\mu_3$ -OH is 1.955(2) Å and the Cu– $\mu_3$ -OH–Cu angle is 115.55(8)°, consistent with weaker bonds to three copper centers.

Among the four dianionic phosphate ligands, three bind to the three Cu(II) ions in a [3.111] coordination mode and the axial phosphate ligand binds to six Cu(II) ions in a [6.222] coordination mode (Harris notation)<sup>48</sup> (see Chart S1 in the ESI<sup>†</sup>), if the weak interaction with the trinuclear motif is included. All phosphate dianions are involved in generating

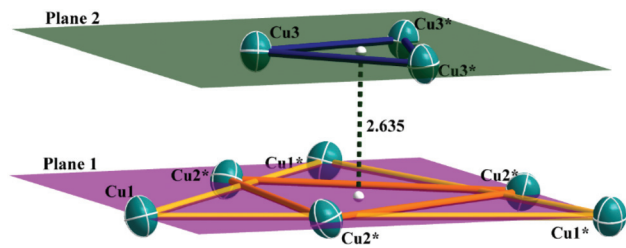


Fig. 6 Mean plane analysis for compound  $2^{\text{MeAr}}$ .

and connecting two layers of Cu(II) ions (Fig. 6). As mentioned above, among the nine Cu(II) ions, six possess distorted square planar geometry and reside in one plane (plane 1) which is supported by four of the phosphate dianions and three pyrazolate ligands. The remaining three Cu(II) ions form a plane (plane 2) parallel to the previous one. The centroid to centroid distance between plane 1 and plane 2 is 2.635(5) Å (Fig. 6).

Compared to compounds  $2^{\text{MeAr}}$ ,  $2^{\text{EtAr}}$  and  $2^{\text{iPrAr}}$ , which possess similar structural features, compound  $2^{\text{Dip}}$  is structurally slightly different. The latter has additional DMF molecules in its crystal lattice and crystallizes in a less symmetric space group. While the gross structural features of  $2^{\text{Dip}}$  are similar to those discussed above, in its trinuclear motif, one of the Cu(II) centers is in closer proximity (2.72 Å) to the oxygen atom of DMF solvent, while the other two are not. As a result, one Cu(II) centre is in a six-coordinate distorted octahedral environment with two rather weakly coordinated axial ligands (Cu–O 2.72 Å for DMF and 2.53 Å for the apical phosphate). This coincides with the apical phosphate ligand being slightly tilted in comparison to the other three compounds. The plane through the three oxygen atoms of the apical phosphate which point towards the trinuclear moiety is perfectly coplanar with the plane through the respective three copper centres (the angle between the planes is 0°) in complexes  $2^{\text{MeAr}}$ ,  $2^{\text{EtAr}}$  and  $2^{\text{iPrAr}}$ . In  $2^{\text{Dip}}$  the angle between those planes is 10.28°. This effectively lowers the overall molecular symmetry resulting in a less symmetric crystallographic space group and in the possibility of fully refining the organic substituent on top, which in the other three complexes had to be removed from the refinement due to exceptionally severe disorder problems. Among the remaining two Cu(II) centres of the trinuclear motif, one is four-coordinate (distorted square-planar), while the other is five-coordinate (distorted square pyramidal) with Cu–O distances to the closest oxygen atom of the apical phosphate of 2.93 Å (no bond) and 2.51 Å (weak bond), respectively (see ESI†). In  $2^{\text{Dip}}$ , the three terminal phosphate dianions hold the three Cu(II) ions in a [3.111] mode of coordination as in the other three structures, but the axial phosphate ligand holds six of the Cu(II) ions in a distinct [5.221] mode of coordination.

All four compounds show intramolecular H-bonding interactions between  $\mu$ -OH (donor) and phosphate oxygen atoms (acceptor) (ESI Fig. S6 and Table S2†). The O...H distances are 1.917(2), 1.938(2) and 1.974 Å in  $2^{\text{MeAr}}$ ,  $2^{\text{EtAr}}$  and  $2^{\text{iPrAr}}$  respectively (ESI Table S2†). Due to the lower crystallographic sym-

metry  $2^{\text{Dip}}$  exhibits three distinctly strong intramolecular H-bonding interactions between  $\mu$ -OH and phosphate oxygen atoms with O...H distances of 2.007(4), 1.943(5), and 1.981(6) Å. The  $\mu_3$ -OH is further involved in intermolecular H-bonding with the oxygen atom of the proximal DMF molecule with an O...H distance of 1.980 Å. The Cu...Cu separations in the skeleton and distances between the planes in  $2^{\text{MeAr}}$ ,  $2^{\text{EtAr}}$ ,  $2^{\text{iPrAr}}$ , and  $2^{\text{Dip}}$  are given in Table S1.† Selected bond lengths, bond angle parameters and the corresponding coordination geometry of all Cu(II) centres in  $2^{\text{MeAr}}$ ,  $2^{\text{EtAr}}$ ,  $2^{\text{iPrAr}}$ , and  $2^{\text{Dip}}$  are given in Tables S3–S6.‡

## Magnetism and EPR

Magnetic susceptibility data for  $2^{\text{MeAr}}$ ,  $2^{\text{EtAr}}$ ,  $2^{\text{iPrAr}}$  and  $2^{\text{Dip}}$  were measured at 0.1, 0.1, 1.0 and 1.0 T applied fields, respectively in the 300–2 K temperature range. The data are shown in Fig. 7 as  $\chi T$  vs.  $T$  plots. The  $\chi T$  products for  $2^{\text{MeAr}}$ ,  $2^{\text{EtAr}}$ ,  $2^{\text{iPrAr}}$  and  $2^{\text{Dip}}$  at 300 K have values of 1.16, 1.13, 1.09 and 1.63 cm<sup>3</sup> K mol<sup>-1</sup>, respectively. These values are much lower than the expected value for nine d<sup>9</sup> Cu(II) ions with  $g = 2.0$  and  $S = 1/2$ . As temperature decreases, the  $\chi T$  product decreases indicating strong antiferromagnetic interactions between the metal centers. As explained in the crystallographic description, the structure of the Cu<sub>9</sub> complexes can be described as two units, Cu<sub>6</sub> and Cu<sub>3</sub>, linked by phosphate ligands; the coupling is depicted as  $J(\text{OPO})'$  in Scheme 2. The Cu<sub>6</sub> unit is in turn formed by three Cu<sub>2</sub> units with NN-pyrazole and OH-bridges; the coupling is shown as  $J(\text{NN})$  in Scheme 2. The three Cu<sub>2</sub> units are linked by phosphates; the coupling is shown as  $J(\text{OPO})$  in Scheme 2. It is known that magnetic exchange through the phosphates will be much smaller than exchange through NN-pyrazole bridging ligands and also antiferromagnetic, and thus the Cu<sub>6</sub> ring is antiferromagnetically coupled. In the trinuclear Cu<sub>3</sub> motif the three Cu(II) centres are bridged by a  $\mu_3$ -OH and pyrazolates; the coupling is shown as  $J(\text{NN})'$  in Scheme 2. For  $2^{\text{MeAr}}$ ,  $2^{\text{EtAr}}$  and  $2^{\text{iPrAr}}$  the three Cu(II)

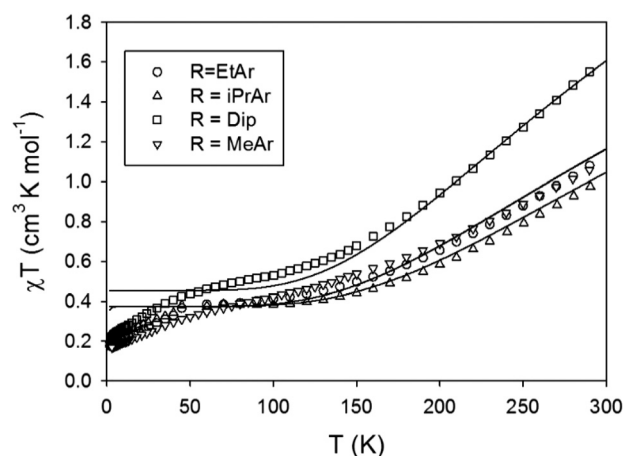
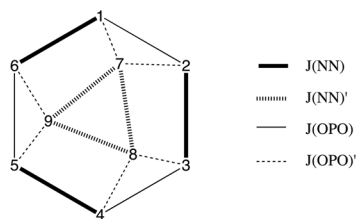


Fig. 7  $\chi T$  product vs.  $T$  plot for  $\chi T$  products for  $2^{\text{MeAr}}$ ,  $2^{\text{EtAr}}$ ,  $2^{\text{iPrAr}}$  and  $2^{\text{Dip}}$ . The solid lines are a simulation of the high-temperature data using the spin Hamiltonian from Scheme 2.



$$\mathcal{H} = -J(NN)[\hat{S}_1\hat{S}_6 + \hat{S}_2\hat{S}_3 + \hat{S}_4\hat{S}_5] - J(NN)'[\hat{S}_7\hat{S}_8 + \hat{S}_8\hat{S}_9 + \hat{S}_7\hat{S}_9] - J(OPO)[\hat{S}_1\hat{S}_2 + \hat{S}_3\hat{S}_4 + \hat{S}_5\hat{S}_6] - J(OPO)'[\hat{S}_1\hat{S}_7 + \hat{S}_2\hat{S}_7 + \hat{S}_3\hat{S}_8 + \hat{S}_4\hat{S}_8 + \hat{S}_5\hat{S}_9 + \hat{S}_6\hat{S}_9]$$

**Scheme 2** Scheme of the magnetic coupling pathways in complexes  $2^{\text{MeAr}}$ ,  $2^{\text{EtAr}}$ ,  $2^{\text{iPrAr}}$ , and  $2^{\text{Dip}}$ .

ions in the  $\text{Cu}_3$  unit are crystallographically equivalent. This results in the antiferromagnetic coupling of the three  $d^9$  centers that is necessarily frustrated in this trinuclear unit, leading to a degenerate spin ground state per trinuclear motif and, hence also for the  $\text{Cu}_9$  complex with  $S = 1/2$ . For  $2^{\text{Dip}}$ , the symmetry is lower and the trinuclear unit can be described as an isosceles triangle that should result in the lifting of a degenerate state necessary for spin frustration. In practice, the two exchange constants in the isosceles triangle will have very large values and will be antiferromagnetic, leading also to a frustrated spin ground state of  $S = 1/2$  for the  $\text{Cu}_9$  complex. In the literature there are abundant references where such NN bridging between two metal centres is part of a pyrazole, triazole,<sup>49–53</sup> or pyridazine<sup>54</sup> ligand. These types of ligands have been used a lot in Cu(II) complexes, since they usually afford effective exchange pathways for antiferromagnetic coupling.<sup>55–59</sup>

For complexes with two Cu–NN–Cu bridges from pyrazole, Bu and Ribas showed that the geometry of the Cu–NN/NN–Cu moiety was the determining factor for the coupling constant  $J$ : the Cu–N–N–Cu torsion angles were all between  $0$  and  $15^\circ$  and the exchange constants had values as large as  $-211 \text{ cm}^{-1}$ .<sup>58</sup> In the complexes reported here the Cu–OH–Cu angles are *ca.*  $115^\circ$  for the trimeric motifs, while the Cu–N–N–Cu torsion angles are between  $0.04^\circ$  and  $8.9^\circ$ . Thus, strong antiferromagnetic coupling is expected for  $J(\text{NN})$  and  $J(\text{NN})'$ , and following the magnetostructural correlation proposed in ref. 62a the exchange constants should be around  $-200 \text{ cm}^{-1}$ . Very strong antiferromagnetic coupling is indeed observed experimentally. The susceptibility data can be modelled with the Hamiltonian obtained from Scheme 2 for  $T > 50 \text{ K}$ . Below this temperature the spin frustration in the equilateral ( $2^{\text{MeAr}}$ ,  $2^{\text{EtAr}}$ , and  $2^{\text{iPrAr}}$ ) or isosceles ( $2^{\text{Dip}}$ ) trinuclear unit must be accounted for. For these calculated susceptibilities the values used were  $g(2^{\text{MeAr}}) = 2.0$ ,  $J(\text{NN}) = J(\text{NN})' = -230 \text{ cm}^{-1}$ ,  $J(\text{OPO}) = J(\text{OPO})' = -4 \text{ cm}^{-1}$ ;  $g(2^{\text{EtAr}}) = 2.0$ ,  $J(\text{NN}) = J(\text{NN})' = -230 \text{ cm}^{-1}$ ,  $J(\text{OPO}) = J(\text{OPO})' = -5 \text{ cm}^{-1}$ ;  $g(2^{\text{iPrAr}}) = 2.0$ ,  $J(\text{NN}) = J(\text{NN})' = -250 \text{ cm}^{-1}$ ,  $J(\text{OPO}) = J(\text{OPO})' = -6.8 \text{ cm}^{-1}$  and  $g(2^{\text{Dip}}) = 2.2$ ,  $J(\text{NN}) = -215 \text{ cm}^{-1}$ ,  $J(\text{NN})' = -215, -215, -120 \text{ cm}^{-1}$ , and  $J(\text{OPO}) = J(\text{OPO})' = -5.8 \text{ cm}^{-1}$ . When fittings are attempted several solutions with different parameters can be obtained.

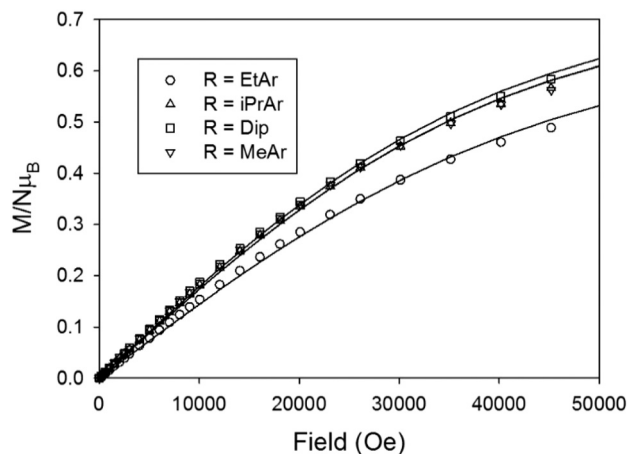


**Fig. 8** Magnetization vs. field plots for  $2^{\text{MeAr}}$ ,  $2^{\text{EtAr}}$ ,  $2^{\text{iPrAr}}$  and  $2^{\text{Dip}}$  at 2 K. The solid lines are fittings of the experimental data.

Magnetization vs. field plots are shown in Fig. 8. The magnetization does not reach saturation at 5 T. In fact the values observed are below the expected value of 1 for an  $S = 1/2$  spin. This implies an effective  $g$  value of less than 2.

The degenerate  $S = 1/2$  in the  $\text{Cu}_9$  complexes is well isolated from the first excited states, with energy differences that range from  $500 \text{ cm}^{-1}$  for  $2^{\text{iPrAr}}$  to  $200 \text{ cm}^{-1}$  for  $2^{\text{Dip}}$ . The magnetization data at 2 K were fitted using the software PHI.<sup>60</sup> This is a typical example of a spin frustrated system, since the three Cu ions Cu7, Cu8 and Cu9 in Scheme 1 are equivalent for  $2^{\text{MeAr}}$ ,  $2^{\text{EtAr}}$ , and  $2^{\text{iPrAr}}$  (equilateral triangle arrangement) and thus the three  $J(\text{NN})'$  values are equal. For  $2^{\text{Dip}}$  (isosceles triangle due to lower symmetry) there should be two  $J(\text{NN})'$  values but these would be similar in magnitude and sign. The magnetization vs. field data at 2 K for  $2^{\text{MeAr}}$ ,  $2^{\text{EtAr}}$ ,  $2^{\text{iPrAr}}$  and  $2^{\text{Dip}}$  were fitted using an isolated  $S = 1/2$  model with an effective  $g$  value. The best fittings are shown as solid lines in Fig. 8 and were obtained for  $g(2^{\text{MeAr}}) = 1.45$ ,  $g(2^{\text{EtAr}}) = 1.32$ ,  $g(2^{\text{iPrAr}}) = 1.45$  and  $g(2^{\text{Dip}}) = 1.47$ . Loss and co-workers proposed that spin–electric coupling is possible in antiferromagnetic ground-state manifolds of  $S = 1/2$  triangles even in the absence of spin–orbit coupling.<sup>61</sup> The low temperature susceptibility values are not as expected from the Curie law for an isolated  $S = 1/2$ , and in turn the  $\chi T$  product decreases linearly and does not extrapolate to zero at  $T = 0 \text{ K}$  but to a value between  $0.1$  and  $0.2 \text{ cm}^3 \text{ K mol}^{-1}$ . This has been observed before in  $\text{Cu}_3$  trinuclear complexes and is attributed to antisymmetric exchange interactions.<sup>62</sup> The antisymmetric exchange can be explained by the orbital overlap between the  $d(x^2 - y^2)$  magnetic orbital of each Cu in the  $\text{Cu}_3$  unit (Cu7, Cu8 and Cu9) with the empty orbitals excited by spin–orbit coupling ( $d_{xy}$ ,  $d_{xz}$ , and  $d_{yz}$ ) on the neighboring Cu(II) ions.<sup>63</sup> The exchange pathway in the reported complexes is effective, since the Cu–Cu distance in the trinuclear unit is  $3.3 \text{ \AA}$ . Effective antisymmetric exchange pathways are reported for Cu–Cu distances as long as  $4.8 \text{ \AA}$ .<sup>63</sup>

Owing to the poor solubility of the compounds, it was not possible to record their EPR spectra in solution. The X-band

EPR spectra of two representative compounds  $2^{\text{Dip}}$  and  $2^{\text{iPrAr}}$  (Fig. S15 and S16 in ESI†) were recorded in the solid state at  $-175\text{ }^{\circ}\text{C}$ . Unfortunately, severe line-broadening possibly due to dipolar interactions limits the amount of information that can be extracted out of these spectra. However, there are certain features that are apparent. The spectra of both the compounds are very similar. The  $g_{\parallel}$  (2.47 and 2.48 for  $2^{\text{Dip}}$  and  $2^{\text{iPrAr}}$ ) values are larger than  $g_{\perp}$  (2.09 and 2.01 for  $2^{\text{Dip}}$  and  $2^{\text{iPrAr}}$ ), and this fact indicates that the unpaired electron in the Cu(II) centers is in the  $d_{x^2-y^2}$  orbital. In addition, “half-field” signals are observed at  $g = 4.34$  and  $g = 4.36$  for  $2^{\text{Dip}}$  and  $2^{\text{iPrAr}}$ , indicating the existence of a multi-spin system.

### UV/vis and luminescence studies

The UV/vis spectra of  $\text{Cu}_9$ ,  $2^{\text{MeAr}}$ ,  $2^{\text{EtAr}}$ ,  $2^{\text{iPrAr}}$  and  $2^{\text{Dip}}$  recorded in DMF ( $10^{-4}\text{ M}$ ) show weak absorption bands at 630–660 nm due to the spin-forbidden d–d transitions of the  $d^9\text{ Cu}^{2+}$  ion and the corresponding  $\epsilon$  values are 530, 445, 530 and 479  $\text{L mol}^{-1}\text{ cm}^{-1}$  respectively (see Fig. S8 in the ESI†). Highly intense absorption bands for  $2^{\text{MeAr}}$ ,  $2^{\text{EtAr}}$ ,  $2^{\text{iPrAr}}$  and  $2^{\text{Dip}}$  appear at 260 nm and are due to ligand-centered  $\pi \rightarrow \pi^*$  transitions with corresponding  $\epsilon$  values of 30 361, 34 639, 36 133 and 21 272  $\text{L mol}^{-1}\text{ cm}^{-1}$  respectively. Intense bands are observed at 309 and 306 nm for  $2^{\text{MeAr}}$  and  $2^{\text{Dip}}$  and a shoulder at around 300 nm for  $2^{\text{EtAr}}$  and  $2^{\text{iPrAr}}$  with  $\epsilon$  of 16 524, 14 412, 16 262 and 15 243  $\text{L mol}^{-1}\text{ cm}^{-1}$  respectively, which are assigned to LMCT.

The photophysical studies of all ligands and the corresponding Cu-complexes were carried out in DMF at ambient temperature. Excitation has been performed at 270 nm for ligands and at two wavelengths 270 nm and 315 nm for the Cu-complexes (see Fig. S9–S11 in the ESI†). Upon excitation at 270 nm  $1^{\text{MeAr}}$ ,  $1^{\text{EtAr}}$ , and  $1^{\text{iPrAr}}$  exhibit an intense emission band at around 300 nm and  $1^{\text{Dip}}$  at 290 nm because of ligand centered emission (LC excited state) (see Fig. S11 in the ESI†). On the other hand,  $2^{\text{MeAr}}$ ,  $2^{\text{EtAr}}$ , and  $2^{\text{iPrAr}}$  exhibit an intense emission band at 304–310 nm upon excitation at 270 nm, because of ligand centered emission (LC excited state) and a weak emission band at 415 nm which could be due to LMCT or a mixed LMCT/LC excited state. In contrast to others, upon excitation at 270 nm  $2^{\text{Dip}}$  displays two intense emissions at 295 and 415 nm. On the other hand, upon excitation at 315 nm,  $2^{\text{MeAr}}$ ,  $2^{\text{EtAr}}$ ,  $2^{\text{iPrAr}}$  and  $2^{\text{Dip}}$  exhibit an intense emission at 417 nm and a weak emission at 348 nm.

The luminescence lifetime measurements of the ligands and their corresponding Cu-complexes were carried out based on the nanosecond time-correlated single photon counting (TCSPC) method (see Fig. S12 and S13 in the ESI†). The lifetimes of the ligands were found to vary between 4.5 and 5.2 ns with the maximum lifetime being encountered for ligand  $1^{\text{Dip}}$  (5.2 ns) (see Table S8 in the ESI†). The slight increase of the lifetime of  $1^{\text{Dip}}$  presumably is due to the absence of the flexible  $\text{CHPh}_2$  group at the *ortho* position of the ligand, which may set off a non-radiative decay process by involving itself in steric crowding. Much to our surprise, all compounds except  $2^{\text{Dip}}$  exhibit almost the same lifetime (4.7–8.5 ns) as their corres-

ponding ligands, ruling out any interference from the paramagnetic metal Cu(II). The slight increase of the lifetime of  $2^{\text{Dip}}$  could be the combined result of a subtle structural change and the absence of any bulky groups at the *ortho* position of the ligand. In view of the relatively poor lifetimes of the ligands and the compounds, we have not attempted to estimate the quantum yields of these systems.

## Experimental

### General procedure

Compounds  $1^{\text{MeAr}}$ ,<sup>46</sup>  $1^{\text{EtAr}}$ ,<sup>46</sup>  $1^{\text{iPrAr}}$ ,<sup>46</sup> and  $1^{\text{Dip}}$ <sup>64</sup> were synthesized according to previously described literature methods. Commercially available starting precursors such as CuCl (Avra synthesis Pvt. Ltd) and pyrazole (Avra synthesis Pvt. Ltd) were used as received. UV/vis spectra were obtained on a Jasco V-670 spectrometer using quartz cells with a path length of 0.1 cm. Fluorescence measurements were carried out on a JASCO FP 8500 spectrometer. Luminescence lifetime measurements were carried out by using a time-correlated single photon counting setup from Horiba Jobin–Yvon. The luminescence decay data were collected on a Hamamatsu MCP photomultiplier (R3809) and were analyzed by using IBH DAS6 software. The electronic absorption and luminescence spectral behaviours of all ligands and their corresponding  $\text{Cu}_9$ -complex compounds were investigated in DMF solvent at  $10^{-4}\text{ (M)}$  concentration. IR spectra were recorded on a Bruker-Alpha spectrometer. Melting points were recorded using Stuart SMP 10 melting point apparatus. Elemental analyses of the compounds were performed on a ThermoQuest CE instrument CHNS-O, the EA/1110 model, and a PerkinElmer Series-II 2400 Elemental Analyzer. Thermogravimetric analyses (TGA) were carried out at a ramp rate of  $10\text{ }^{\circ}\text{C min}^{-1}$  under a flow of nitrogen using a Discovery TGA by the TA Instruments-Waters Lab. Melting points were recorded using Stuart SMP 10 melting point apparatus. EPR spectra at X-band frequency (*ca.* 9.5 GHz) were obtained with a Magnettech MS-5000 benchtop EPR spectrometer equipped with a rectangular TE 102 cavity. The measurements were carried out in synthetic quartz glass tubes.

### X-ray crystallography

Single crystal X-ray diffraction data for  $2^{\text{MeAr}}$  and  $2^{\text{EtAr}}$  were collected at low temperature ( $-103.0\text{ }^{\circ}\text{C}$ ) using an STOE-IPDS 2 T diffractometer with graphite-monochromatic molybdenum  $K\alpha$  radiation,  $\lambda = 0.71073\text{ \AA}$ . The structure was solved by direct methods using WINGX<sup>65</sup> and SHELXL<sup>66</sup> programs and refined by full matrix least-squares methods based on  $F^2$ . All non-hydrogen-atoms were refined with anisotropic displacement parameters. The hydrogen atoms were refined isotropically on calculated positions using a riding model with their  $U_{\text{iso}}$  values constrained to  $1.5U_{\text{eq}}$  of their pivot atoms for terminal  $\text{sp}^3$  carbon atoms and 1.2 times for the aromatic carbon atoms. Single crystal X-ray data for  $2^{\text{iPrAr}}$  were collected on a Super Nova Dual source X-ray Diffractometer system (Agilent Technologies) equipped with a CCD area detector and oper-

ated at 250 W power (50 kV, 0.8 mA) to generate Mo K $\alpha$  radiation ( $\lambda = 0.71073 \text{ \AA}$ ) and Cu K $\alpha$  radiation ( $\lambda = 1.54178 \text{ \AA}$ ) at 298 (2) K. The linear absorption coefficients, scattering factors for the atoms, and the anomalous dispersion corrections were taken from International Tables for X-ray crystallography.<sup>67</sup> Data integration and reduction were processed with SAINT software.<sup>68</sup> An empirical absorption correction was applied to the collected reflections with SADABS<sup>69</sup> using XPREP.<sup>70</sup> The structure was solved by direct methods using WINGX<sup>65</sup> and SHELXL<sup>66</sup> programs and refined by full matrix least-squares methods based on  $F^2$ . Hydrogens were fixed in their ideal geometries, and their contributions were included in the refinement. The single crystal X-ray data for  $2^{\text{Dip}}$  were collected on a Bruker APEX-II CCD diffractometer using graphite-monochromatic Mo K $\alpha$  radiation ( $\lambda = 0.71073 \text{ \AA}$ ).

The structures of  $2^{\text{MeAr}}$ ,  $2^{\text{EtAr}}$ , and  $2^{\text{iPrAr}}$  exhibited the same problem which constitutes a peculiar case of disorder. The organic substituent on the apical PO<sub>4</sub> moiety is so severely disordered by rotation around the P–O bond pointing towards the substituent (which is exactly on a threefold rotation axis of the trigonal space group) that it was impossible to model or even refine the disorder at all. Instead of refining the structure in the trigonal space group it was also tested whether the disorder would disappear when the structure was refined in a less symmetric space group (even down to  $P\bar{1}$ ) and whether the cell could be expanded to accommodate more than six molecules. The same severe disorder was, however, still present in all of these trials.

The structure was also carefully tested for twinning, albeit without any success. The problem apparently is that there is this 3-fold axis applicable for the whole rest of the Cu<sub>9</sub> clusters but this axis cannot be applied to the organic substituent on top which has a 2-fold symmetry at best (depending on the orientation/nature of the aliphatic substituent on top of the phenyl ring). This substituent can therefore acquire in principle three to six different orientations with respect to the threefold axis and in the structure we observe an overlap of all atoms belonging to these distinct orientations. Because it was impossible to assign these atoms to chemically reasonable positions it was decided not to refine this substituent but to apply the SQUEEZE/PLATON routine and remove the respective electron density from the refinement.<sup>71</sup> The routines yielded void volumes and electron counts which were in accordance with the removed substituents (276–322 electrons per formula). The unrefined substituents were included in the respective sum formulae, hence, leading to discrepancies between experimental and theoretical formulae and the respective alerts in the checkcif file.

In the case of  $2^{\text{Dip}}$ , four molecules of DMF did co-crystallize (one coordinated to Cu) lowering the overall symmetry of the structure to  $P\bar{1}$  and here the apical substituent could be refined. The DMF molecules were however disordered and all four were refined with EADP constraints (individually for each solvent molecule).

All crystallographic data were deposited with the Cambridge Crystallographic Data Centre. CCDC 1835295 ( $2^{\text{MeAr}}$ ), 1835294 ( $2^{\text{EtAr}}$ ), 1835296 ( $2^{\text{iPrAr}}$ ), and 1835293 ( $2^{\text{Dip}}$ ).<sup>‡</sup>

## Magnetic measurements

Magnetic measurements were carried out at the Unitat de Mesures Magnètiques (Universitat de Barcelona) on polycrystalline samples (*circa* 30 mg) with a Quantum Design SQUID MPMS-XL magnetometer equipped with a 5 T magnet. Diamagnetic corrections were made using Pascal's constants and an experimental correction for the sample holder was applied.

## Synthetic procedures

**The Synthesis of  $2^{\text{MeAr}}$ ,  $2^{\text{EtAr}}$ ,  $2^{\text{iPrAr}}$ , and  $2^{\text{Dip}}$ .** The following general synthetic protocol was used to prepare these complexes: ArOP(O)(OH)<sub>2</sub> (Ar = 2,6-(CHPh)<sub>2</sub>-4-R-C<sub>6</sub>H<sub>2</sub>; R = Me ( $1^{\text{MeAr}}$ ), Et ( $1^{\text{EtAr}}$ ), iPr ( $1^{\text{iPrAr}}$ ) and Ar = 2,6-diisopropylphenyl ( $1^{\text{Dip}}$ )) (1.6 mmol) was added as a solid to the CH<sub>3</sub>CN (160 mL) solution of CuCl (0.36 g, 3.6 mmol). A pale yellow turbid solution was obtained. Pyrazole (0.16 g, 2.4 mmol) followed by Et<sub>3</sub>N (0.8 mL, 5.6 mmol) was added to the yellow turbid solution. A deep blue turbid solution was obtained immediately. The reaction was allowed to stir for 20 h at room temperature. Then 32 mL of DMF was added to it and stirred for 1 h with gentle warming. Then, the resultant deep blue solution was filtered and the filtrate was kept for crystallization. Deep blue block shaped crystals were obtained. The yields, melting points and the IR characterization data for the products are provided below:

$2^{\text{MeAr}}$ . Yield: 0.84 g, 62%. M. P.: 222 °C. IR (KBr pellet, cm<sup>-1</sup>):  $\nu = 3442$  (s), 3084 (w), 3059 (w), 3026 (w), 2929 (w), 2862 (w), 1953 (w), 1642 (vs), 1600 (w), 1554 (w), 1493 (w), 1446 (w), 1382 (w), 1283 (w), 1254 (w), 1208 (w), 1145 (m), 1133 (m), 1106 (m), 1052 (m), 1032 (w), 1004 (m), 920 (w), 896 (w), 855 (w), 761 (w), 713 (m), 702 (m), 626 (w), 605 (w), 649 (w), 524 (w), 459 (vs), 440 (m), 430 (m), 423 (m), 406 (m). Anal. calcd for C<sub>159</sub>H<sub>151</sub>Cu<sub>9</sub>N<sub>15</sub>O<sub>23</sub>P<sub>4</sub>: C, 57.25; H, 4.56; N, 6.30. Found: C, 56.53; H, 4.51; N, 6.69.

$2^{\text{EtAr}}$ . Yield: 0.79 g, 58%. M. P.: 229 °C. IR (KBr pellet, cm<sup>-1</sup>):  $\nu = 3444$  (s), 3084 (w), 3059 (w), 3026 (w), 2963 (w), 2932 (w), 2872 (w), 1950 (w), 1642 (s), 1600 (w), 1493 (w), 1447 (w), 1382 (w), 1322 (w), 1282 (w), 1254 (w), 1206 (w), 1147 (m), 1132 (m), 1105 (m), 1052 (m), 1032 (w), 1003 (m), 938 (w), 919 (w), 888 (w), 859 (w), 761 (w), 713 (m), 702 (m), 626 (w), 605 (w), 592 (w), 524 (w), 482 (w), 473 (w), 456 (s), 447 (vs), 420 (s), 405 (m). Anal. calcd for C<sub>163</sub>H<sub>159</sub>Cu<sub>9</sub>N<sub>15</sub>O<sub>23</sub>P<sub>4</sub>: C, 57.72; H, 4.73; N, 6.19. Found: C, 56.51; H, 4.68; N, 6.72.

$2^{\text{iPrAr}}$ . Yield: 0.9 g, 65%. M. P.: 224 °C. IR (KBr pellet, cm<sup>-1</sup>):  $\nu = 3444$  (s), 3083 (w), 3059 (w), 3026 (w), 2959 (w), 2933 (w), 2870 (w), 1949 (w), 1641 (vs), 1601 (w), 1493 (m), 1468 (w), 1446 (w), 1383 (w), 1365 (w), 1319 (w), 1282 (w), 1257 (w), 1209 (w), 1147 (s), 1127 (s), 1105 (s), 1052 (s), 1032 (w), 1004 (s), 921 (w), 903 (w), 854 (w), 791 (w), 761 (w), 714 (s), 701 (s), 663 (w), 649 (w), 626 (w), 605 (w), 593 (w), 561 (w), 529 (w), 492 (w), 475 (w), 456 (s), 444 (w), 426 (s), 411 (m). Anal. calcd for C<sub>167</sub>H<sub>167</sub>Cu<sub>9</sub>N<sub>15</sub>O<sub>23</sub>P<sub>4</sub>: C, 58.17; H, 4.88; N, 6.09. Found: C, 57.03; H, 4.80; N, 6.51.

$2^{\text{Dip}}$ . Yield: 0.84 g, 84%. M. P.: 223 °C. IR (KBr pellet, cm<sup>-1</sup>):  $\nu = 3464$  (s), 3135 (w), 3063 (w), 3023 (w), 2963 (m), 2935 (w),

2868 (w), 1644 (vs), 1489 (w), 1466 (w), 1438 (w), 1382 (w), 1362 (w), 1338 (w), 1282 (w), 1257 (w), 1176 (w), 1142 (vs), 1105 (vs), 1050 (vs), 1003 (vs), 913 (s), 882 (w), 801 (w), 767 (s), 695 (w), 662 (w), 627 (w), 602 (w), 544 (m), 485 (w), 460 (m), 441 (s), 422 (w), 410 (w). Anal. calcd for  $[C_{78}H_{118}Cu_9N_{16}O_{24}P_4]$ : C, 39.70; H, 5.04; N, 9.50. Found: C, 39.21; H, 4.86; N, 9.15.

## Conclusions

In this contribution, we report the synthesis and characterization of highly symmetric  $Cu_9$ -phosphates that have been assembled by using bulky phosphate monoesters along with pyrazole co-ligands. A novel feature of all four enneanuclear  $Cu(II)$  phosphates described herein is that the  $Cu_9$  core is made up of two distinct  $Cu_6$  and  $Cu_3$  motifs. These two motifs are stitched together by the bridging coordination action of three mono-phosphate ester ligands. While all three  $Cu(II)$  centres in the trinuclear unit are bridged together by a  $\mu_3$ -OH, each pair within this unit is bridged by a pyrazole ligand. The hexanuclear unit contains three dinuclear  $Cu(II)$  motifs connected to each other by phosphate ligands. Within the dinuclear motif, the two  $Cu(II)$  centers are bridged by an -OH and a pyrazole ligand. Magnetic studies reveal a strong antiferromagnetic exchange between the  $Cu(II)$  centres of the dinuclear units in the hexanuclear part and a strong spin frustration in the trinuclear part leading to a degenerate ground state.

## Conflicts of interest

There are no conflicts to declare.

## Acknowledgements

This project was funded by intramural funds at Tata Institute of Fundamental Research (TIFR) Hyderabad, Gopanally, Hyderabad-500107, Telangana, India from the Department of Atomic Energy (DAE), Government of India, India. VC thanks the Department of Science and Technology, New Delhi, India, for a National J. C. Bose fellowship. We are thankful to the Department of Chemistry, IIT Kanpur, Kanpur, India for HRMS and elemental analysis data. We are thankful to Subhrajyoti Dolai, TIFR Hyderabad for fluorescence measurements. ECS acknowledges financial support from the Spanish Government (Grant CTQ2015-68370-P). We are also thankful to Prof. Rahul Banerjee, IISER Kolkata, India for the single-crystal X-ray data for  $2^{IPFAR}$ . We are grateful to the reviewers for their critical insights to improve the quality of the manuscript.

## References

- 1 C. Alvarez, R. Llavona, J. R. Garcia, M. Suajrez and J. Rodriguez, *Inorg. Chem.*, 1987, **26**, 1045–1049.
- 2 S. W. Martin, *J. Am. Ceram. Soc.*, 1991, **74**, 1767–1784.
- 3 Y. Nishiyama, S. Tanaka, H. W. Hillhouse, N. Nishiyama, Y. Egashira and K. Ueyama, *Langmuir*, 2006, **22**, 9469–9472.
- 4 B. Z. Tian, X. Y. Liu, B. Tu, C. Z. Yu, J. Fan, L. M. Wang, S. H. Xie, G. D. Stucky and D. Y. Zhao, *Nat. Mater.*, 2003, **2**, 159–163.
- 5 A. K. Sahu, S. Pitchumani, P. Sridhar and A. K. Shukla, *Fuel Cells*, 2009, **9**, 139–147.
- 6 T. Y. Ma, X. J. Zhang and Z. Y. Yuan, *Microporous Mesoporous Mater.*, 2009, **123**, 234–242.
- 7 G. J. Hutchings, *J. Mater. Chem.*, 2004, **14**, 3385–3395.
- 8 Y. Wang, X. X. Wang, Z. Su, Q. Guo, Q. H. Tang, Q. H. Zhang and H. L. Wan, *Catal. Today*, 2004, **93**, 155–161.
- 9 R. H. Lin, Y. J. Ding, L. F. Gong, W. D. Dong, J. H. Wang and T. Zhang, *J. Catal.*, 2010, **272**, 65–73.
- 10 Z. Y. Yuan, T. Z. Ren, A. Azioune, J. J. Pireaux and B. L. Su, *Catal. Today*, 2005, **105**, 647–654.
- 11 J. Yu, A. Wang, J. Tan, X. Li, J. A. van Bokhoven and Y. K. Hu, *J. Mater. Chem.*, 2008, **18**, 3601–3607.
- 12 A. Sarkar and P. Pramanik, *Microporous Mesoporous Mater.*, 2009, **117**, 580–585.
- 13 X. S. Li, A. R. Courtney, W. Yantasee, S. V. Mattigod and G. E. Fryxell, *Inorg. Chem. Commun.*, 2006, **9**, 293–295.
- 14 A. Dutta, A. K. Patra and A. Bhaumik, *Microporous Mesoporous Mater.*, 2012, **155**, 208–214.
- 15 X. Y. Tian, W. He, J. J. Cui, X. D. Zhang, W. J. Zhou, S. P. Yan, X. N. Sun, X. X. Han, S. S. Han and Y. Z. Yue, *J. Colloid Interface Sci.*, 2010, **343**, 344–349.
- 16 L. C. Qian, Y. Xia, W. K. Zhang, H. Huang, Y. P. Gan, H. J. Zeng and X. Y. Tao, *Microporous Mesoporous Mater.*, 2012, **152**, 128–133.
- 17 T. Z. Ren, Z. Y. Yuan, A. Azioune, J. J. Pireaux and B. L. Su, *Langmuir*, 2006, **22**, 3886–3894.
- 18 S. Rodriguez-Liviano, F. J. Aparicio, T. C. Rojas, A. B. Hungria, L. E. Chinchilla and M. Ocana, *Cryst. Growth Des.*, 2012, **12**, 635–645.
- 19 Q. L. Luo, S. D. Shen, G. Z. Lu, X. Z. Xiao, D. S. Mao and Y. Q. Wang, *J. Mater. Chem.*, 2009, **19**, 8079–8085.
- 20 S. V. Kononova and M. A. Nesmeyanova, *Biochemistry*, 2002, **67**, 184–195.
- 21 M. Gielen and E. R. T. Tiekink, *Metallotherapeutic Drugs and Metal-Based Diagnostic Agents: The Use of Metals in Medicine*, John Wiley & Sons, Ltd., 2005.
- 22 T. W. Kim, P. W. Chung, I. I. Slowing, M. Tsunoda, E. S. Yeung and V. S. Y. Lin, *Nano Lett.*, 2008, **8**, 3724–3727.
- 23 J. W. Liu, A. Stace-Naughton, X. M. Jiang and C. J. Brinker, *J. Am. Chem. Soc.*, 2009, **131**, 1354–1355.
- 24 A. C. Kalita, N. Gogoi, R. Jangir, S. Kuppaswamy, M. G. Walawalkar and R. Murugavel, *Inorg. Chem.*, 2014, **53**, 8959–8969.
- 25 S. K. Gupta, A. A. Dar, T. Rajeshkumar, S. Kuppaswamy, S. K. Langley, K. S. Murray, G. Rajaraman and R. Murugavel, *Dalton Trans.*, 2015, **44**, 5961–5961.
- 26 S. Konar, P. S. Mukherjee, E. Zangrando, F. Lloret and N. R. Chaudhuri, *Angew. Chem., Int. Ed.*, 2002, **41**, 1561–1563.

- 27 E. I. Tolis, M. Helliwell, S. Langley, J. Raftery and R. E. P. Winpenny, *Angew. Chem., Int. Ed.*, 2003, **42**, 3804–3808.
- 28 E. K. Brechin, R. A. Coxall, A. Parkin, S. Parsons, P. A. Tasker and R. E. P. Winpenny, *Angew. Chem., Int. Ed.*, 2001, **40**, 2700–2703.
- 29 S. Langley, M. Helliwell, J. Raftery, E. I. Tolis and R. E. P. Winpenny, *Chem. Commun.*, 2004, 142–143.
- 30 V. Chandrasekhar, D. Sahoo, R. S. Narayanan, R. J. Butcher, F. Lloret and E. Pardo, *Dalton Trans.*, 2013, **42**, 8192–8196.
- 31 J. A. Sheikh, H. S. Jena, A. Clearfield and S. Konar, *Acc. Chem. Res.*, 2016, **49**, 1093–1103.
- 32 R. Murugavel, M. G. Walawalkar, M. Dan, H. W. Roesky and C. N. R. Rao, *Acc. Chem. Res.*, 2004, **37**, 763–774.
- 33 L. Zhu, O. Santos, C. W. Koo, M. Rybstein, L. Pape and J. W. Canary, *Inorg. Chem.*, 2003, **42**, 7912–7920.
- 34 T. Gajda, A. Jancso, S. Mikkola, H. Lönnberg and H. Sirges, *J. Chem. Soc., Dalton Trans.*, 2002, 1757–1763.
- 35 L. M. Rossi, A. Neves, A. J. Bortoluzzi, R. Hoerner, B. Szpoganicz, H. Terenzi, A. S. Mangrich, E. Pereira-Maia, E. E. Castellano and W. Haase, *Inorg. Chim. Acta*, 2005, **358**, 1807–1822.
- 36 R. Murugavel, S. Kuppaswamy, A. N. Maity and M. P. Singh, *Inorg. Chem.*, 2009, **48**, 183–192.
- 37 R. Murugavel, M. Sathiyendiran, R. Pothiraja, M. G. Walawalkar, T. Mallah and E. Rivière, *Inorg. Chem.*, 2004, **43**, 945–953.
- 38 S. Sabiah, B. Vargheseb and N. N. Murthya, *Chem. Commun.*, 2009, 5636–5638.
- 39 R. Murugavel, S. Kuppaswamy, A. N. Maity and M. P. Singh, *Inorg. Chem.*, 2009, **48**, 183–192.
- 40 B. M. Ahmed and G. Mezei, *Inorg. Chem.*, 2016, **55**, 7717–7728.
- 41 C. K. Hartman and G. Mezei, *Inorg. Chem.*, 2017, **56**, 10609–10624.
- 42 G. Mezei, P. Baran and R. G. Raptis, *Angew. Chem., Int. Ed.*, 2004, **43**, 574–577.
- 43 V. Chandrasekhar, L. Nagarajan, R. Cleérac, S. Ghosh and S. Verma, *Inorg. Chem.*, 2008, **47**, 1067–1073.
- 44 V. Chandrasekhar, T. Senapati, A. Dey and E. C. Sañudo, *Inorg. Chem.*, 2011, **50**, 1420–1428.
- 45 V. Chandrasekhar and L. Nagarajan, *Dalton Trans.*, 2009, 6712–6714.
- 46 D. Mandal, B. Santra, P. Kalita, N. Chrysochos, A. Malakar, R. S. Narayanan, S. Biswas, C. Schulzke, V. Chandrasekhar and A. Jana, *ChemistrySelect*, 2017, **2**, 8898–8910.
- 47 A. Escuer, G. Vlahopoulou, S. P. Perlepes and F. A. Mautner, *Inorg. Chem.*, 2011, **50**, 2468–2478.
- 48 R. A. Coxall, S. G. Harris, D. K. Henderson, S. Parsons, P. A. Tasker and R. E. P. Winpenny, *J. Chem. Soc., Dalton Trans.*, 2000, 2349.
- 49 C. Y. Su, Y. Z. Tong, F. C. Yuan, Q. L. Wang, Y. Ma, G. M. Yang and D. Z. Liao, *Inorg. Chim. Acta*, 2014, **423**, 545–549.
- 50 G. Novitchi, W. Wernsdorfer, L. F. Chibotaru, J.-P. Costes, C. E. Anson and A. K. Powell, *Angew. Chem., Int. Ed.*, 2009, **48**, 1614–1619.
- 51 Y. L. Bai, V. Tangoulis, R. B. Huang, L. S. Zheng and J. Tao, *Chem. – Eur. J.*, 2009, **15**, 2377–2383.
- 52 W. Mazureck, B. J. Kennedy, J. R. Rodgers, K. S. Murray, M. J. O'Connor, J. R. Rodgers, M. R. Snow, A. G. Wedd, P. R. Zwack and R. Peter, *Inorg. Chem.*, 1985, **24**, 3258–3264.
- 53 G. A. Craig, M. Schu, D. Aguila, O. Roubeau, J. Ribas-arín, S. Vela, S. J. Teat and G. Arom, *Inorg. Chem.*, 2014, **53**, 3290–3297.
- 54 L. K. Thompson, S. K. Mandal, E. J. Gabe, F. L. Lee and A. W. Addison, *Inorg. Chem.*, 1987, **26**, 657–664.
- 55 S. Fustero, M. Sánchez-Roselló, P. Barrio and A. Simón-Fuentes, *Chem. Rev.*, 2011, **111**, 6984–7034.
- 56 M. Du, S.-T. Chen, Y.-M. Guo, X.-H. Bu and J. Ribas, *J. Mol. Struct.*, 2005, **737**, 17–21.
- 57 T.-L. Hu, J.-R. Li, C.-S. Liu, X.-S. Shi, J.-N. Zhou, X.-H. Bu and J. Ribas, *Inorg. Chem.*, 2006, **45**, 162–173.
- 58 M. Mohan, M. R. Bond, T. Otieno and C. J. Carrano, *Inorg. Chem.*, 1995, **34**, 1233–1242.
- 59 V. Chandrasekhar, A. Dey, T. Senapati and E. C. Sañudo, *Dalton Trans.*, 2012, **41**, 799–803.
- 60 N. F. Chilton, R. P. Anderson, L. D. Turner, A. Soncini and K. S. Murray, *J. Comput. Chem.*, 2013, **34**, 1164–1175.
- 61 M. Trif, F. Troiani and D. Stepanenko, *Phys. Rev. B: Condens. Matter Mater. Phys.*, 2010, **82**, 1–29.
- 62 (a) S. Ferrer, F. Lloret, E. Pardo, J. M. Clemente-Juan, M. Liu-González and S. García-Granda, *Inorg. Chem.*, 2012, **51**, 985–1001; (b) A. Escuer, G. Vlahopoulou, F. Lloret and F. A. Mautner, *Eur. J. Inorg. Chem.*, 2014, **2014**, 83–92.
- 63 E. T. Spielberg, A. Gilb, D. Plaul, D. Geibig, D. Hornig, D. Schuch, A. Buchholz, A. Ardavan and W. Plass, *Inorg. Chem.*, 2015, **54**, 3432–3438.
- 64 G. M. Kosolapoff, C. K. Arpke, R. W. Lamb and H. Reich, *J. Chem. Soc. C*, 1968, 815–818.
- 65 L. J. Farrugia, WinGX and ORTEP for Windows: an update, *J. Appl. Crystallogr.*, 2012, **45**, 849–854.
- 66 G. M. Sheldrick, *SHELXL-97, Program for Crystal Structure Refinement*, University of Göttingen, Göttingen, Germany, 1997.
- 67 *International Tables for X-Ray Crystallography*, Kynoch Press, Birmingham, England, 1952, vol. **III**.
- 68 *SAINT+*, version 6.02, Bruker AXS, Madison, WI, 1999.
- 69 G. M. Sheldrick, *SADABS, Empirical Absorption Correction Program*, University of Göttingen, Germany, 1997.
- 70 *XPREP*, Siemens Industrial Automation Inc., Madison, WI, 5.1 edn, 1995.
- 71 A. L. Spek, PLATON SQUEEZE: A Tool for the Calculation of the Disordered Solvent Contribution to the Calculated Structure Factors, *Acta Crystallogr., Sect. C: Struct. Chem.*, 2015, **71**, 9–18.